by R. Allenspach

Spin-polarized scanning electron microscopy

In this paper, a review is presented of a powerful technique for studying magnetic microstructures: spin-polarized scanning electron microscopy, denoted as spin-SEM. or SEMPA. When the beam of a scanning electron microscope traverses a ferromagnetic sample, secondary electrons are emitted whose spin polarization contains information on the magnitude and direction of the magnetization of the surface. Various illustrative examples are presented which describe the main features of the technique, such as its very high surface sensitivity, its suitability for achieving complete separation of relevant magnetic and topographic information, and its high lateral resolution.

1. Introduction

Ferromagnetism has several remarkable features, but probably the most intriguing one is that a small external magnetic field can induce a huge change of the magnetization state. This "amplification" can be as large as 10⁵ and has attracted considerable interest for more than one hundred years. It was Weiss [1] who proposed a solution to this riddle in 1907 with his concept of magnetic domains. Weiss postulated that a ferromagnet decays into areas in which the magnetization points along a well-defined axis, but that the magnetization direction can change by large angles from area to area. By averaging

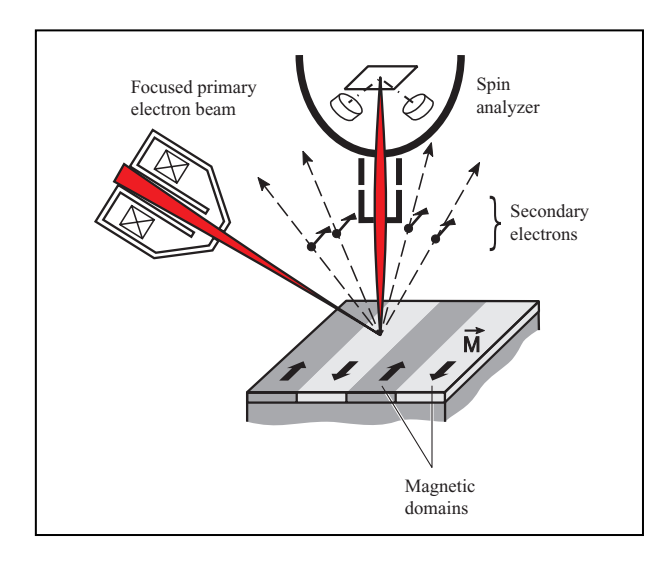
over all domains in a ferromagnetic specimen, one can achieve almost any remanent magnetization, depending on the history of the sample. No techniques existed to verify Weiss's domain concept until 1931, when Bitter [2] and von Hámos and Thiessen [3] independently proposed a technique to indicate the presence of magnetic domains. They predicted that with the dispersion of a magnetic powder on a ferromagnetic surface, the fine magnetic particles should assemble at positions where the magnetic stray field leaks out of the surface, i.e., at domain walls. The agglomeration of these particles is then observed with an optical microscope. However, another two decades elapsed before the domain pattern on an Fe single crystal was observed [4] by the so-called Bitter technique, which verified the concept proposed by Weiss.

Since then, various methods have been developed for the observation of magnetic domains. Of course, each has advantages as well as disadvantages. An overview of domain-imaging methods has recently been published [5].

This review covers a domain-imaging technique called spin-polarized scanning electron microscopy (spin-SEM, or SEMPA) that is particularly suitable for investigating ultrathin ferromagnetic films [6–9]. Its greatest strength lies in its very high surface sensitivity, making it ideal for investigating phenomena related to magnetism in thin or ultrathin films. Interestingly, the technique was originally developed to observe magnetic domains and domain walls of bulk samples with high resolution under "realistic" conditions, i.e., without the need to thin specimens as in transmission electron microscopy. It has been

©Copyright 2000 by International Business Machines Corporation. Copying in printed form for private use is permitted without payment of royalty provided that (1) each reproduction is done without alteration and (2) the Journal reference and IBM copyright notice are included on the first page. The title and abstract, but no other portions, of this paper may be copied or distributed royalty free without further permission by computer-based and other information-service systems. Permission to republish any other portion of this paper must be obtained from the Editor.

0018-8646/00/\$5.00 © 2000 IBM



Schematic illustration of the spin-SEM principle. An unpolarized, focused electron beam is scanned across a ferromagnetic surface, and the spin polarization of the emitted secondary electrons, a measure of the surface magnetization, is determined by a spin analyzer.

applied to enhance our understanding of domain patterns in amorphous as well as crystalline materials, for fundamental studies on the origin of ferromagnetism in two-dimensional systems as well as for investigating technologically relevant problems such as the imaging of written bits or the performance of write heads in magnetic storage.

Section 2 describes and illustrates the relevant aspects of the technique. In subsequent sections, examples demonstrate the use of spin-SEM to investigate basic problems in ferromagnetism and selected applied topics.

2. Technique

The use of spin-polarized secondary electrons for magnetic domain viewing was suggested by DiStefano in 1978 [10]. Interestingly, the main goal was to fabricate a beam-addressed memory device based on an electron gun and spin detector. The first working instrument was built by Koike and Hayakawa [11], who combined an electron gun having a 10- μ m-diameter beam with a spin detector to visualize magnetic domains on Fe(100) single crystals. Shortly afterward, Unguris et al. [12] used an ultrahigh-vacuum SEM with an attached home-built spin analyzer to image magnetic domain patterns. Since then, two acronyms exist for the same method: Spin-SEM was chosen by Koike et al., whereas the term SEMPA—scanning electron microscopy with polarization analysis—was coined by Unguris et al.

In the meantime, various such systems have been built. To our knowledge there are currently eight running dedicated microscopes located at laboratories throughout the world. They differ primarily in the type of spin detector used for the polarization analysis and in the magnetization components they are able to determine. In addition, each of the systems has further specific tools attached, such as the capability to anneal or cool the sample during imaging, to apply magnetic fields, to perform reflection high-energy electron diffraction (RHEED) for structural characterization, or to investigate surface morphology by scanning tunneling microscopy.

All of these systems provide a comprehensive characterization of the magnetic samples under investigation, and several examples illustrate the strengths of the technique. In this section, we concentrate on its experimental aspects.

The spin-SEM or SEMPA technique is a straightforward extension of standard scanning electron microscopy (SEM); see Figure 1. Use is made of a scanning electron microscope equipped with a spin-polarization detector. As in SEM, a finely focused beam of high-energy electrons is scanned across the surface of a sample. The electrons scatter at the electrons in the near-surface region of the sample in various different ways. The predominant process is inelastic scattering: An incoming primary electron transfers some of its energy to an electron of the sample. In most cases, upon scattering, the electron loses only a small amount of energy. This process occurs repeatedly until it has essentially lost its energy and a cascade of excited low-energy secondary electrons has been created. A considerable number of these secondary electrons travel back to the surface and are ejected into vacuum, the number depending on the local curvature of the surface. Hence, an image of the sample topography is obtained by recording the number of these electrons for each position of the incoming beam. If the sample under investigation is ferromagnetic, the emitted electrons are spin-polarized. The spin of these secondary electrons points preferentially in the opposite direction of the magnetization vector. Thus, by measuring the spin polarization along a certain direction in space, a map of the magnetization component in this direction is obtained.

The spin polarization of the secondary electrons is strongly dependent on the secondary electron energy, as indicated in **Figure 2**. The polarization at higher energies is the one expected from the spin imbalance of the bands near the Fermi level. However, at very low energies it peaks at a value typically two to three times that expected from the imbalance. This enhancement at very low energies is attributed to preferential inelastic scattering of \downarrow spin electrons, which leads to a higher escape probability for \uparrow spin electrons. Since the intensity of secondary electrons is also highest at the lowest energies,

an efficient instrument for magnetic-domain imaging collects the abundance of electrons from a relatively large energy window (typically 0 to 10 eV) with their high spin polarization. In fact, it is this advantageous combination of high intensity and polarization enhancement that allows us to image magnetic patterns in ultrathin films only a few atomic layers thick.

The crucial part of the method involves measuring the spin polarization of the secondary electrons. Various spin detectors have been developed in recent decades. The physical principle behind most of them is to use spin-orbit interaction as a means of transforming a spin asymmetry into a spatial asymmetry. In a Mott detector [13], for instance, the electrons are accelerated to high energies (typically 50 to 100 keV) and scattered by a high-atomicnumber target such as a thin Au foil. This scattering is spin-dependent because of the spin-orbit interaction. Therefore, electrons with \uparrow and \downarrow spin with respect to the scattering plane are preferentially scattered into different directions. The spin polarization P is then determined from the number $N \uparrow$ and $N \downarrow$ of electrons counted in a pair of detectors located at the angle of maximum scattering asymmetry:

$$P = (N \uparrow - N \downarrow)/(N \uparrow + N \downarrow). \tag{1}$$

In all currently used spin analyzers, at least one additional detector pair is positioned such that a second polarization component along an orthogonal axis is measured at the same time. This can either be the second in-plane magnetization component, or, as in our system, the perpendicular component. By measuring all three magnetization components, a vectorial map of the magnetization can be produced, which is very valuable for specimens having complicated domain structures.

Other detector types, such as the LEED detector [14] or the low-energy diffuse scattering detector [12], use the same physical principle, but make use of scattering at much smaller energies (of the order of 100 eV). The efficiency of all of these detectors is notoriously low. In general, the figure of merit of a spin detector is of the order of 10⁻⁴ [15]. The spin analyzer employed in our system is a Mott-type detector operated at 100 keV. It has a spherically focusing electrical field which efficiently minimizes spurious apparatus asymmetries. These asymmetries originate from variations of the beam position and the angle of incoming electrons as well as from manufacturing tolerances. Given the inherently low efficiency of spin analyzers, domain imaging involves a constant struggle for a greater flux of electrons. Therefore, considerable effort has been invested in designing the electron optics at the entrance of the spin detector. Apart

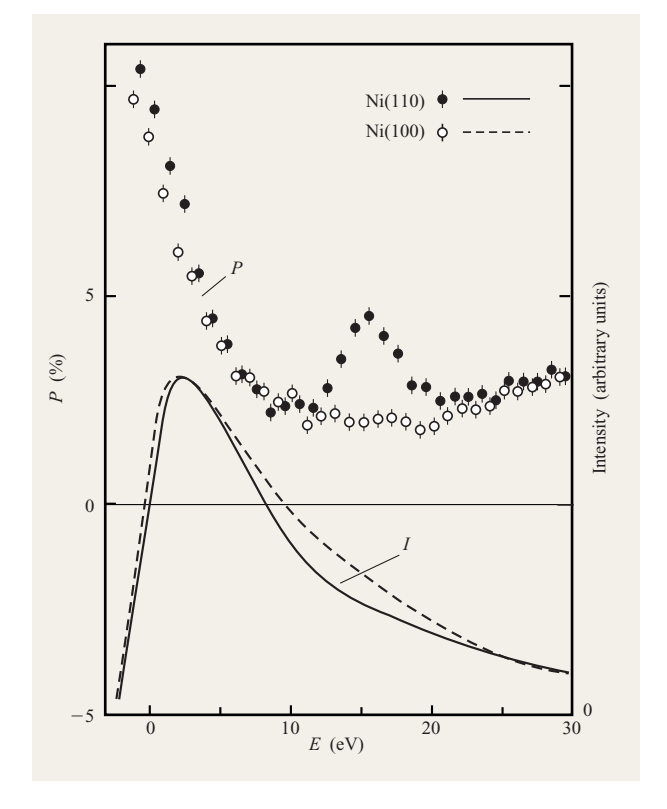


Figure 2

Secondary-electron spin polarization P and intensity I vs. kinetic energy of secondary electrons from Ni(100) and Ni(110), recorded at a primary-electron energy of 600 eV. Note the large polarization enhancement at low kinetic energies. Similar enhancements occur for the other 3d transition-metal ferromagnets Fe and Co, with peak values of $\sim 50\%$ and $\sim 35\%$, respectively. The polarization peak at 16 eV in Ni(110) is a signature of the spin-polarized band structure for this particular crystallographic orientation.

from the energy selection and acceleration stages, one to several beam-steering plates are necessary to collect all of the available electrons, transport them to the spin analyzer, and focus them at the scattering target. The low efficiency of spin detection is the experimental constraint of spin-SEM. Therefore, electron-beam sources having a high brightness, such as field-emitter sources, are used. Nevertheless, spin-SEM is a "slow" technique because image acquisition takes several minutes.

A significant advantage of spin-SEM over most other magnetic imaging techniques follows from Equation (1): Spin polarization is a normalized quantity, independent of changes in the total number $N=N\uparrow+N\downarrow$ of electrons emitted. Therefore, fluctuations of the incoming beam current and the emitted secondary electrons do not show up in the magnetization images. The topographic map without magnetic information is obviously given directly

¹ M. Landolt, unpublished work.

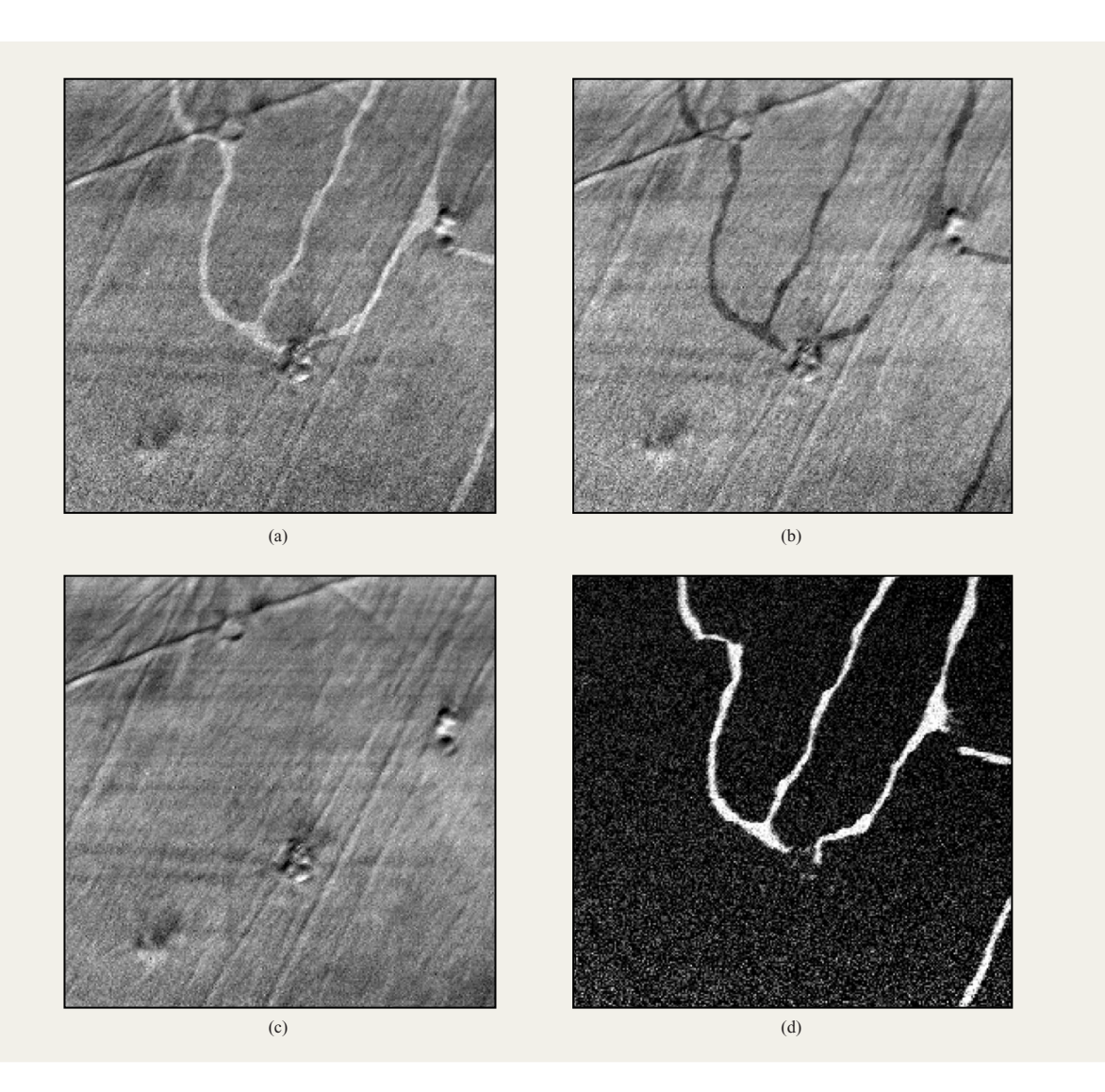


Image reconstruction in spin-SEM illustrated by the use of a 3-ML fcc-Fe/Cu(100) film. The two detector signals $N\dagger$ and $N\dagger$ of the perpendicular polarization component are shown in (a) and (b), respectively. The topography (i.e., the sum of both electron counters $N\dagger + N\dagger$) is shown in (c), and the perpendicular polarization [i.e., $(N\dagger - N\dagger)/(N\dagger + N\dagger)$] is shown in (d). From the black/white contrast in (d), it is concluded that the magnetization was perpendicular and pointing mainly in the negative direction (black). Several reversed domains (white) are visible. Note that the topography and magnetization are completely separated. The detector signals show that the domains were pinned at defects of the Cu substrate. The simultaneously acquired in-plane polarization component (not shown) was homogeneously gray; i.e., the film was fully magnetized out-of-plane. The beam parameters for this image were primary energy of 2 keV and beam current <1 nA; the data acquisition time was 50 ms per pixel, and the image area was 150 μ m × 150 μ m.

by N, as in standard SEM operation. Thus, spin-SEM not only gives both topography and magnetic information simultaneously, but completely separates the two, as is illustrated in **Figure 3**. An ultrathin Fe film three monolayers (ML) thick was epitaxially grown on Cu(100). Owing to the high surface anisotropy, this film was perpendicularly magnetized [16]. The image deduced from

the counters measuring the perpendicular polarization hence displays oppositely magnetized domains as black/white contrast. In the corresponding topography map, several defects are visible in the substrate that do not show up in the magnetic image. In fact, it can be concluded from the individual counter signals that these defects actually pin the domains.

This first example shows one of the most prominent features of the technique, its high surface sensitivity. Only a few techniques exist that are able to image magnetic domains in ultrathin films near the Curie temperature. The reason for this sensitivity is the short probing depth of spin-SEM, which is determined by the small inelastic mean free path of the secondary electrons. Whereas the incoming high-energy primary beam typically penetrates the sample to a depth of several hundred nanometers, the traveling distance of a low-energy secondary electron is of the order of 1 nm in 3d ferromagnets [17] because of the many scattering channels available. Because of this high surface sensitivity, clean, uncovered surfaces are required for domain imaging by spin-SEM. Therefore, an ultrahighvacuum environment is necessary. The short probing depth, on the other hand, also means that the very surface is imaged even in bulk samples. This fact has led, for instance, to the discovery that a domain wall in a bulk ferromagnet such as Fe(100), which is of a Bloch wall type, is terminated as a Néel wall at the top surface [18, 19].

Another feature of spin-SEM is its high lateral resolution. It is governed primarily by the diameter of the probing electron beam at beam currents that are high enough to form a magnetic image having a sufficient signal-to-noise ratio. The magnetic resolution is routinely below 100 nm; i.e., it is superior to that of most other domain-imaging techniques such as classical optical microscopies (magneto-optic Kerr microscopy or the Bitter technique), which are diffraction-limited to several hundred nanometers. Similar resolution is obtained with other electron microscopy techniques, most notably for example spin-polarized low-energy electron microscopy (SPLEEM) [20] and photoelectron emission microscopy when linear or circular dichroism is used to record magnetic information [21, 22]. The latter technique in particular is very promising, with its elemental specificity and its use for imaging antiferromagnets. The technique is described elsewhere in this issue [23]. The only available technique having a better resolution is transmission electron microscopy (Lorentz microscopy, electron holography), which, however, requires sophisticated sample preparation. The best resolution obtained up to now using spin-SEM is 20 nm, which has been achieved by using a higher probe current and modifying the standard electron optics in the SEM, viz., by using a low-aberration objective lens and a short working distance [24].

However, even with these sophisticated improvements the magnetic resolution is still worse than the beam diameter. In our spin-SEM the smallest probe diameter is 5 nm, whereas the best magnetic resolution obtained in a domain wall profile is 40 nm; see **Figure 4**. This figure shows the domain wall in a 50-ML Co/Au(111) film [25]. A cross-tie wall [26] is characterized by an in-plane magnetization rotation of oppositely oriented wall

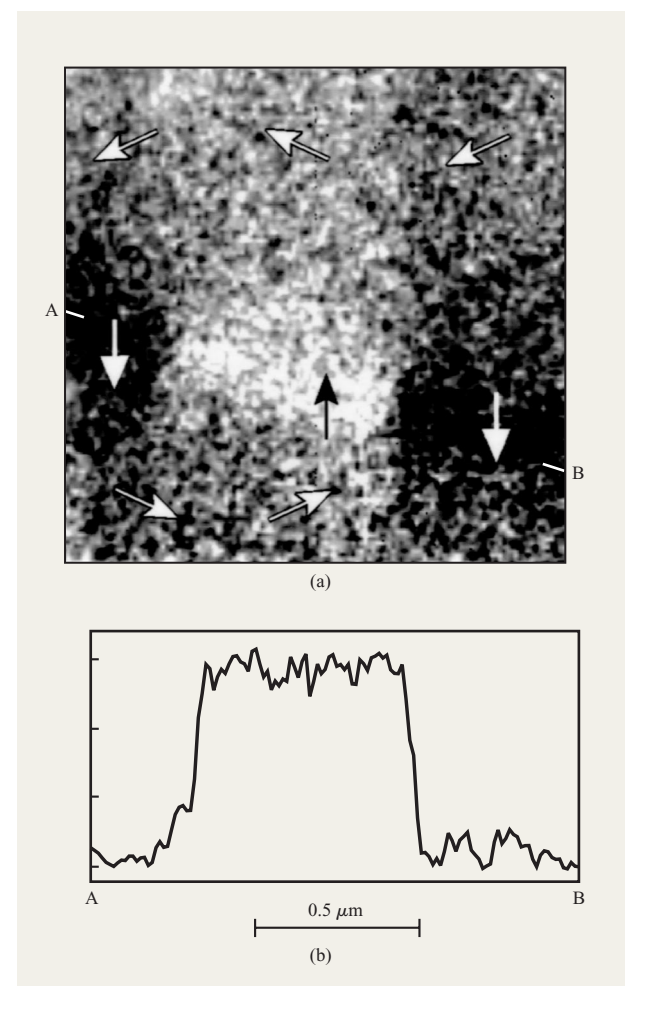


Figure 4

(a) High-resolution image of a domain wall in an in-plane magnetized 50-ML Co film grown on Au(111). The cross-tie wall runs along the line from point A to point B. Three wall segments of opposite magnetization are identified along this line. (b) The line scan shows the sharp transitions between oppositely magnetized segments. The narrower transition was only 40 nm wide. The faint contrast extending into the domains adjacent to the wall [top and bottom of (a)] shows that the magnetization was slightly rotated to avoid magnetic singularities at the wall edges. The scan area was 1.4 $\mu m \times 1.4~\mu m$. Adapted from [25], with permission.

segments, which separate the antiparallel magnetization direction of the adjacent domains. The narrower transition width along the wall was 40 nm, deduced from the line scan in Figure 4. Note that the wall width itself was much larger, of the order of $\sim\!150$ nm. The faint contrast within the domains adjacent to the wall is typical for a cross-tie wall. It signifies a slight magnetization rotation within the plane that closes the flux between oppositely magnetized

wall segments. The asymmetry of the two transitions along the wall is believed to be caused by the asymmetry of flux closure: Although each transition within the wall is a vortex singularity, only every second one produces a spike that influences the adjacent domains. In ultrathin films, cross-tie walls are not expected to occur for energetic reasons [26]. Perpendicularly magnetized ultrathin Co/Au(111) films are expected to have Bloch walls. We were not able to resolve the intrinsic wall width in these films. In our system, resolution is limited by line-frequency electromagnetic interferences. In standard SEM operation, synchronization with line frequency is done routinely. In spin-SEM, the typical electron count accumulation time at each position is of the order of 2 to 100 ms, so the experimental use of line synchronization is not directly applicable. Furthermore, we routinely operate the microscope at beam voltages that are too low for optimum resolution. The primary energy is typically in the range from 1 to 5 keV rather than 25 keV as in standard SEM. The reason for this pertains to the yield of the secondary electrons: For most relevant ferromagnetic metals it has a broad maximum at an energy around 1 keV with values close to 1; hence, the number of secondary electrons available for spin-polarization analysis is maximum at this energy as well.

3. Magnetization imaging on curved surfaces

Today, imaging magnetic domains at the surface of a bulk ferromagnet is a routine task, and magnetization patterns in ultrathin films can also be determined with high resolution and sensitivity. However, imaging magnetic domain patterns on curved surfaces is not at all trivial for most experimental methods. Optical illumination techniques such as the magneto-optic Kerr or Faraday effects often use a 180° reflection of light and suffer from a short focal depth. Hence, in general only part of the image of a curved or sloped surface has an acceptable resolution. Magnetic force microscopy (MFM) [27] is also a scanning probe technique that requires a flat surface because the tip–sample spacing has to be held constant by changing the length of a piezoelectric element, which is usually limited to a submicrometer length scale.

A notable exception is scanning Kerr microscopy [28], provided it is equipped with an automatic focus adjustment capability. This change from an illumination to a scanning technique, however, causes image acquisition to become slow, thus counteracting one of the most attractive features of Kerr microscopy.

In electron microscopy the depth of focus is large, and sharp images can therefore be obtained routinely on strongly curved surfaces. Since spin-SEM obviously has the same characteristics, it is one of the very few techniques that can be used to image magnetic-domain configurations on inclined or curved surfaces. This property has been

used for viewing the magnetic-domain pattern on the side plane of write heads for longitudinal recording [29]. Edge domains at the sides of the heads cause nonreproducible switching responses upon magnetization reversal. It has been found that a multilayer structure is largely able to suppress such domains.

Let us examine, for example, the magnetization pattern on a cone-shaped surface. MFM tips are imaged to identify whether the apex region of the tip is in a singledomain state. In MFM, a ferromagnetic tip attached to a flexible cantilever is immersed in the magnetic stray field of the specimen under investigation. The dipolar force between stray field and tip magnetization is a measure of the magnetization distribution in the sample. The relation between the magnetization distribution and the measured force signal, however, is quite intricate. Assuming a magnetization direction along the tip axis, it has been shown that the length of the apex domain determines whether the tip acts as a dipole or a single pole, and hence whether the force or the force gradient is measured [30]. The transition between these two extreme behaviors is gradual, which often complicates MFM image interpretation, particularly if the magnetization direction of the sample under investigation is not known a priori. Clearly, if the domain configuration in the tip is known, image reconstruction, as proposed for example in References [30] and [31], is more feasible.

A first attempt to investigate the domain configuration in an MFM tip was made using Foucault-mode Lorentz microscopy [31]. With this technique, the position of the domain walls integrated across the tip is determined by measuring the deflection of the probing electrons by the magnetic induction outside of the tip. It has been concluded that Ni tips are in a single-domain state at least for the first 20 μ m from the tip apex. Electron holography has also been applied to determine the magnetic state of MFM tips [32]. Qualitative agreement is obtained with the model of a single-pole Ni tip. Quantitative interpretation is hampered by the fact that the long-range stray field of the tip perturbs the reference electron beam necessary for creating the hologram.

A direct determination of the surface domain configuration of an MFM tip can be made using spin-SEM. The magnetization pattern of an Fe tip is shown in **Figure 5**, together with simultaneously acquired topographic images (to the right). The overview presented in Figure 5(a) proves that the overall magnetization direction at the surface of the tip is along the tip axis, confirming that shape anisotropy plays the dominant role. From the higher-magnification image in Figure 5(b), one might conclude that the apex region is indeed a single-domain state with a length of $>7~\mu$ m. However, an oppositely magnetized domain is pinned at one side next to the apex [Figure 5(c)]. Our results suggest that such

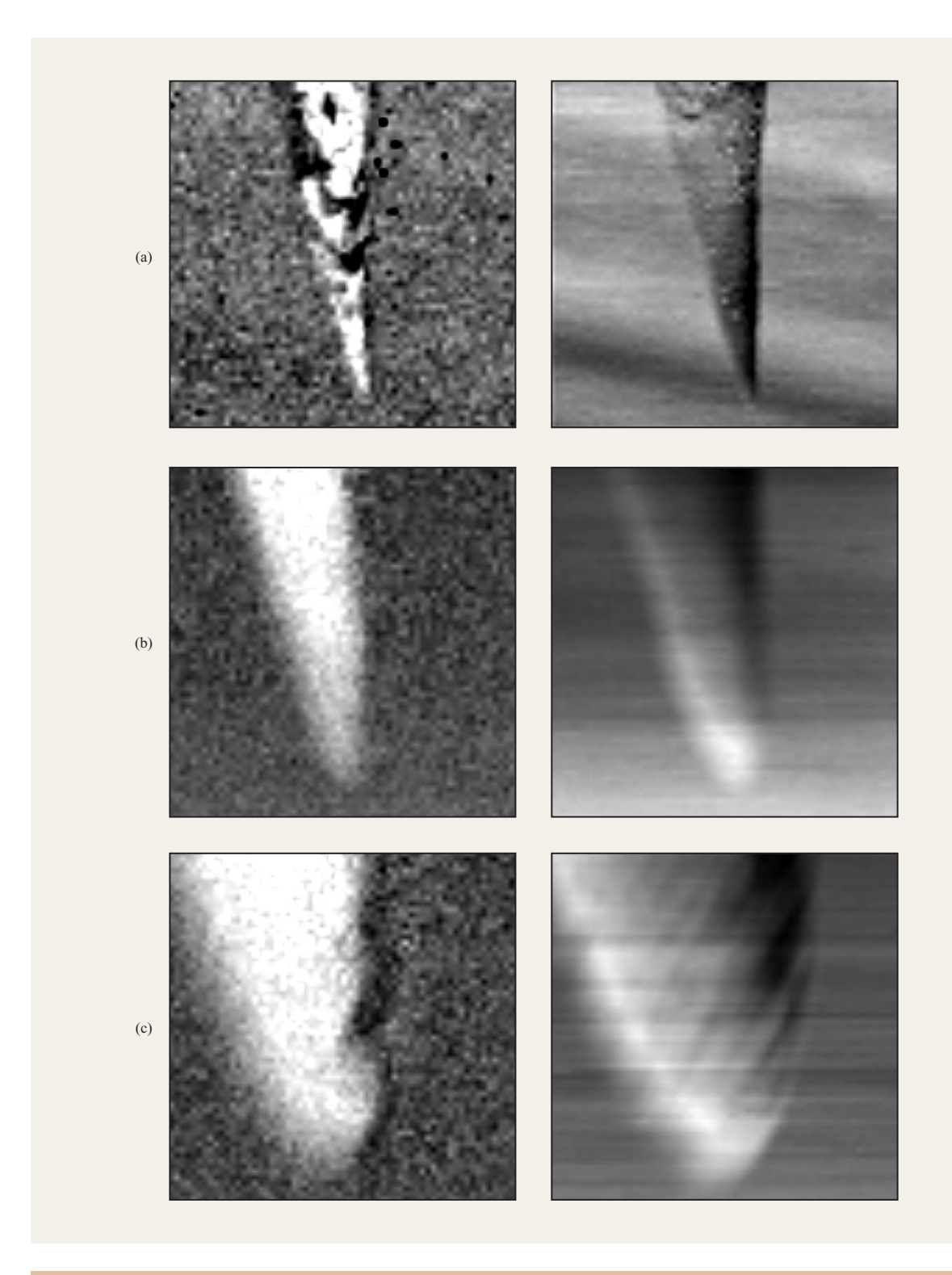


Figure 5

Spin-SEM images of an iron MFM tip, with the measured magnetization direction along the tip axis (left). The simultaneously acquired topographic images (right) showing the cone shape of the tips illustrate that spin-SEM can be used to determine magnetization patterns on curved surfaces. Scan areas were (a) 50 μ m \times 50 μ m, (b) 7.5 μ m \times 7.5 μ m, (c) 2.5 μ m. Note the oppositely magnetized domain at the right-hand side of the tip.

deviations from the expected single-domain state are responsible for the differences in experimental observations of seemingly similar tips.

4. Magnetization reversal in an applied field

In order to study magnetization reversal on a microscopic scale, observation is necessary in the presence of the magnetic field needed to induce the reversal. For an electron spectroscopy such as spin-SEM, this appears to be impossible because low-energy electrons are deflected by magnetic fields owing to the Lorentz force. In this respect, optical techniques such as Kerr microscopy have much less stringent requirements and are thus superior.

However, as discussed later in this section, spin-SEM can be used under favorable circumstances to map domain patterns in an applied field. The applied field is very small but sufficient to study magnetization reversal in a 3-ML Fe/Cu(100) film with perpendicular magnetization. Starting with the single-domain state, an opposing external field of increasing magnitude is applied, and the domain configuration is recorded at each step until the reversed saturated state is reached.

Microscopic studies of magnetization reversal are essentially studies of the imperfections of a specimen: A perfect crystal, whatever its size, should behave like a single-domain particle in which magnetization reversal can occur only by coherent rotation [33]. The reason for this astonishing prediction is that a reverse domain can be nucleated only by rotating the magnetization through 180°. Because the crystal is defect-free, the nucleation field is identical at each point; hence, the magnetization rotates coherently [34]. Apart from the fact that perfect samples exist only in theory, there is also a conceptual flaw in this argument if one considers reversal along the easy magnetization axis. The external field does not exert torque on the magnetization and thus induces no rotation, neither coherent nor incoherent. Therefore, magnetization reversal by rotation is rarely observed in real samples. To our knowledge, it has been identified unequivocally only in specimens too small to support a multidomain state [35].

More realistic types of reversal exist, such as curling, buckling, nucleation of reversed domains, and propagation of domain walls. These different modes affect the macroscopic properties of a ferromagnet. They determine not only the shape of the hysteresis loop but also in particular the coercivity and remanence. A thorough understanding of these quantities therefore requires a study of domain structures and their reaction to magnetic fields in the presence of crystalline imperfections.

This intimate connection between microscopic domains and the macroscopic hysteresis loop was established for the first time by Williams and Shockley in their pioneering work on a picture-frame Fe–Si single crystal [4]. They

demonstrated a quantitative relation between domain-wall motion and a change in magnetization, and observed a hindrance to wall motion at defects at the surface. Since then, a vast number of results have been accumulated for three-dimensional bulk specimens and thick films. Microscopic observations of magnetization reversal in ultrathin films, on the other hand, are rare, owing to the lack of appropriate techniques.

A notable exception is a study of magnetization reversal in perpendicularly magnetized Au/Co/Au(111) layers using magneto-optical Faraday microscopy [36]. The study profited from the fact that Au grows epitaxially on a transparent glass substrate. Two extreme regimes were identified in which reversal is dominated by either domain nucleation or domain-wall motion. The reason for this different behavior of quasi-similar samples is not entirely clear, although it is expected that structural properties play a role [36]. A drawback of Kerr microscopy, the magneto-optical technique in reflection, is that its signalto-noise ratio is poor for ultrathin films. Therefore, its use requires that a reference image of the saturated state be subtracted from each image. This makes a direct observation of magnetization reversal difficult. Nevertheless, it has been used to identify domain-wall motion in ultrathin Pd/Co/Pd(111) and Pt/Co/Pt(111) layers [37, 38]. In Pd/Co/Pd(111) the reversal mode changes above a Co thickness of 8 ML to random nucleation [37].

Let us now look at the application of spin-SEM to investigate the magnetization reversal in a perpendicularly magnetized film in 3-ML fcc-Fe/Cu(100). The macroscopic hysteresis loop obtained using the Kerr effect is compared directly to the domain images measured while an external field H is applied.

The Fe film was grown at T = 90 K and annealed to T = 300 K, as described elsewhere [16]. The hysteresis cycle obtained using the polar Kerr effect is shown in Figure 6(a). The coercive field was small $(H_c = 600 \text{ A/m})$, as expected for a film at a temperature near its Curie temperature. The shape of the loop was almost square, with remanence approaching saturation. In fact, the domain images observed by spin-SEM proved that the remanent state was single-domain throughout, except at a nonmagnetic defect. Figure 6(c) shows the entire magnetization reversal from this uniformly magnetized remanent state to the oppositely magnetized saturated configuration. The images contain a wealth of features, some of which are discussed briefly below. Between H = 437 A/m and 461 A/m, the first reversed domains have nucleated at a scratch visible in topography that runs diagonally across the image [Figure 6(b)]. Wall motion can also be seen, for instance between H = 510 A/mand 544 A/m at the lower right. Then propagation stops: The wall of this particular domain appears to

be pinned to fields of $H=597~{\rm A/m}$. The final reversal of submicrometer-sized "hard" magnetic entities at crystalline defects is seen when the field is increased from $H=728~{\rm A/m}$ to $825~{\rm A/m}$. Note that nucleation centers also appear at locations where no structural defect is observed in the topography, for example at $H=524~{\rm A/m}$ at the lower right. It is likely, however, that there is also a tiny irregularity present. Not only can structural defects in the substrate serve as nucleation sites, but also, for example, a variation in Fe film thickness. Since the perpendicular anisotropy depends critically on film thickness d in the surface anisotropy term $K_{\rm S}/d$, thickness changes affect the magnetic properties locally by causing the microscopic coercive field to vary.

It is interesting that in the presence of such diverse phenomena, the simplest possible magnetization curve is observed, namely, essentially a square loop. In fact, it has been argued [36] that a nucleation-dominated magnetization reversal should lead to a nonrectangular hysteresis loop because of local variations of nucleation and propagation fields, which in turn lead to an H_a distribution. Figure 6 shows that this distribution is rather narrow for the Fe/Cu(100) film, which is consistent with the Kerr hysteresis loop. Indeed, one can prove that the imaged area is representative of the entire sample on the millimeter scale. For each image, the average polarization can be calculated and normalized to the saturated state. As expected, these values are in good agreement with the Kerr loop of Figure 6(a). Moreover, this correspondence rules out the possibility that time-dependent effects [39] play a major role on the time scale of our experiment: The Kerr loop was traced in 2 s, whereas each spin-SEM image required between 80 and 330 s.

Further experiments are necessary to test the different modes of magnetization reversal that occur in ultrathin films. It appears to be established that ultrathin films with the perfection that can be achieved today do not support magnetization rotation. Both domain nucleation and wall propagation occur. The aim is to disentangle these modes by tuning the structural properties of the films until they exhibit the desired magnetic characteristics.

These experiments show that in magnetically soft thin films, spin-SEM can be used to image magnetization reversal on a microscopic scale. The unavoidable stray fields are small enough that the emitted low-energy secondary electrons still reach the spin analyzer.

5. Patterning magnetic anisotropy by electron irradiation

Control of magnetic anisotropy provides a means for investigating basic concepts in low-dimensional magnetic systems as well as a means for tuning magnetic properties for possible applications. A striking effect associated with magnetic anisotropy is the one accompanied by a change

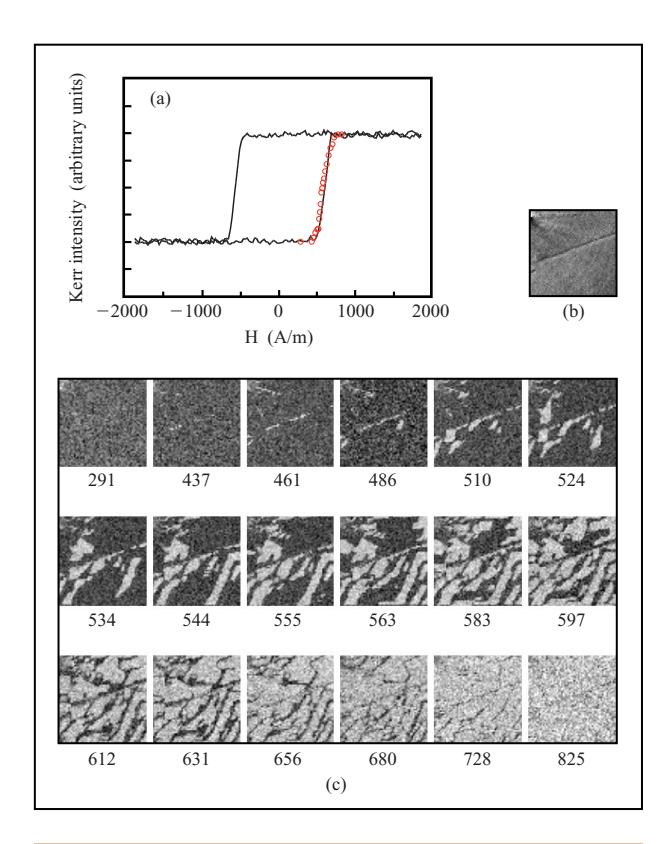
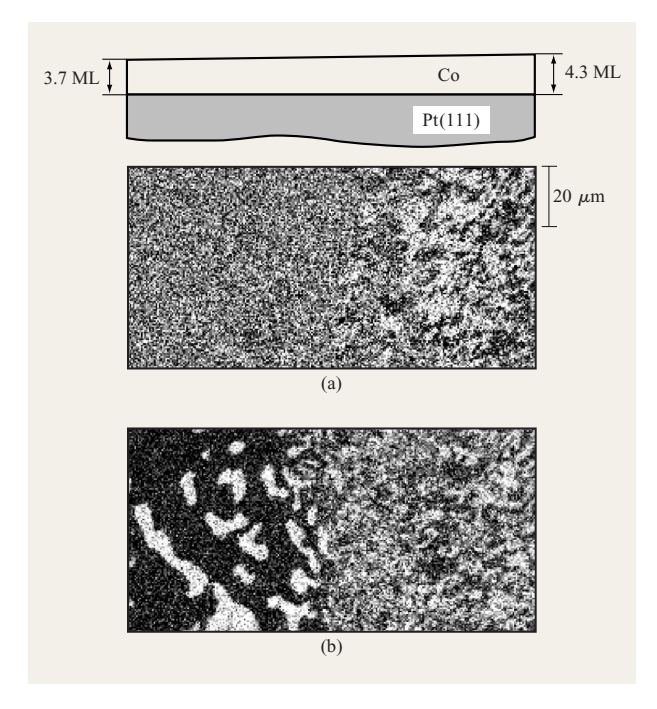


Figure 6

(a) Hysteresis loop obtained from a perpendicularly magnetized 3-ML fcc-Fe/Cu(100) film using the polar Kerr effect. The red circles correspond to the polarization averages over the scan area of the spin-SEM images in (c). (b) Topography of the specimen, showing a defect at the upper left-hand corner and a scratch diagonally across the sample. (c) Series of spin-SEM images (perpendicular magnetization component) displaying the complete magnetization reversal from single-domain remanence to reversed single-domain saturation. The applied external field is indicated at each image in units of A/m. The scan area was 100 $\mu m \times 100~\mu m$. Both nucleation and wall propagation can be identified. For details, see the text.

of the easy magnetization direction. An increase of the perpendicular magnetic surface anisotropy can lead to a complete reorientation of the magnetization from parallel to perpendicular to a film surface. It can be induced by depositing metal layers [40] or by annealing [41]. For Co/Cu films, switching within the film plane can also be induced by chemisorption of gases [42, 43]. Ion etching, on the other hand, has the opposite effect—reducing perpendicular anisotropy [44]. Although film properties have thus been altered on a macroscopic length scale, modifications of the magnetic properties on a local scale have been induced by small amounts of metallic adsorbates [45] and by ion bombardment [46]. The latter experiments are particularly attractive for possible



(a) In-plane and (b) out-of-plane magnetization component of a Co film grown as a wedge onto a Pt(111) substrate. The wedge is sketched above the images, indicating the linear increase of thickness from left to right. Note the gradual transition from fully perpendicular magnetization to a canted magnetization state with domains both in the in-plane and the out-of-plane components. Domain size shrinks as the reorientation thickness is approached.

application in future high-density data-storage devices. Patterned media are expected to be a possible solution to achieve magnetic storage densities beyond foreseen limits [47].

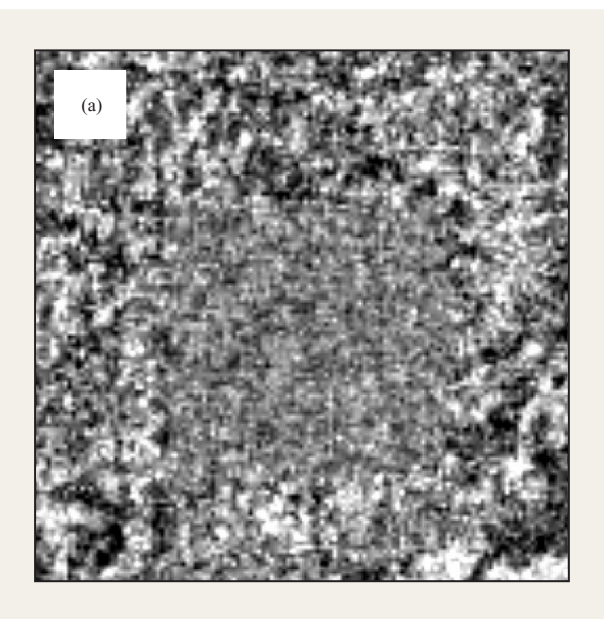
The experiments presented in this section show that modifications on a local scale are possible without adding or removing atoms or molecules. Modified magnetic properties can be "written" into an ultrathin Co film with the electron beam of our SEM. In this way, the magnetization direction can be forced to change locally, and magnetic domain sizes can be expanded by up to one order of magnitude [48]. These results show that both electrons and ions are able to strongly change magnetic anisotropy. We find that electrons, unlike ion irradiation, increase anisotropy. This is particularly attractive because an ideal patterned medium consists of isolated magnetic entities in a nonmagnetic matrix. Increasing anisotropy in small areas is a first step toward patterning a magnetic film by irradiating it through a shadow mask.

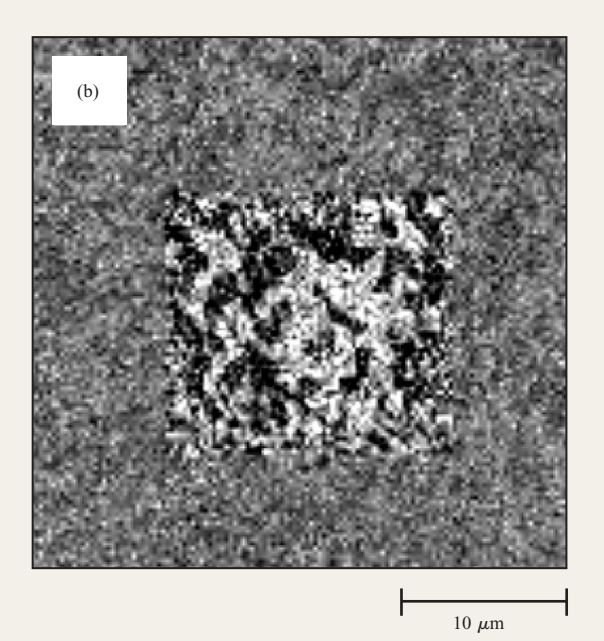
Co films were epitaxially grown onto a Pt(111) single crystal held at room temperature. Owing to the strong

anisotropy of the Co/Pt interface, such films are oriented perpendicularly to the surface. At greater thicknesses, shape anisotropy forces the magnetization direction into the film plane, as indicated in Figure 7. Domain size is observed to shrink in a narrow thickness range near reorientation, as expected theoretically [49] and also as observed experimentally in the Co/Au(111) system [41]. Slightly above the reorientation thickness, a canted magnetization is observed having small domains in both the in-plane and out-of-plane portions. The thickness at which reorientation takes place varies within a wide range and depends on the actual miscut of the surface from the (111) orientation. Films are then grown slightly thicker than the reorientation thickness, i.e., the thickness at which they exhibit in-plane magnetization. For these films one can locally modify the magnetic anisotropy to such an extent that the magnetization reorients to the perpendicular direction. This patterning is achieved by electron irradiation in our spin-SEM.

By removing the objective aperture and reducing condenser coil excitation, the intensity of the 10-keV electron beam is increased to the maximum values attainable in comparison to standard operation. This leads to a beam current of 10 nA at the sample position. Repeated scanning over selected areas of the sample surface then leads to local magnetic modifications, as illustrated in Figure 8. The center square was irradiated with a dose of 2.4×10^{10} electrons/ μ m². A magnetic image subsequently acquired with standard beam parameters at a smaller magnification shows both the electron-beam-treated area and its surroundings. Within the square, the magnetization direction has switched completely from in-plane to out-of-plane, as shown by the uniformly gray level in Figure 8(a) and the black/white contrast in Figure 8(b). The square decays into a demagnetized state of up/down domains having typical sizes of several micrometers. The untreated film, on the other hand, consists of smaller, in-plane magnetized domains.

Our results suggest that electron irradiation improves the film or the interface quality and thus enhances anisotropy. Reduced interface roughness has been identified as one of the causes of an increase in surface anisotropy [50]. Electron bombardment has already been shown to increase exchange coupling across Cr in Fe/Cr/Fe structures [51]. The results were interpreted in terms of a smoothening of the Fe/Cr interface. From their observations of beam voltage and beam-power dependencies, the authors of Reference [51] concluded that a local two-electron process from a core hole must be involved. This process transfers part of the relaxation energy to the lattice either by electron–phonon interaction or by creating a nucleus of a new structural phase. It





Magnetic domain images of a Co/Pt(111) film, obtained by spin-SEM after electron bombardment of a centered square for 1200 s: (a) inplane and (b) out-of-plane magnetization components. The central region has fully changed from being magnetized parallel to being magnetized perpendicularly to the surface. Image size 35 μ m. From [48], with permission.

appears that electron irradiation helps the system evolve toward equilibrium, in contrast to the experiments in Reference [46], where defects are created by ion bombardment.

Direct thermal annealing is disregarded as the cause of the increase in anisotropy because the beam power levels used lead to a temperature rise of less than 0.1 K in the sample [48]. Similarly, one can rule out alloying at the interface [52] because it occurs only for temperatures above 350 K [53]. Film contamination by the electron beam as observed with standard SEM [54] is also ruled out because the contamination level is below the detection limit of our Auger electron spectroscopy system.

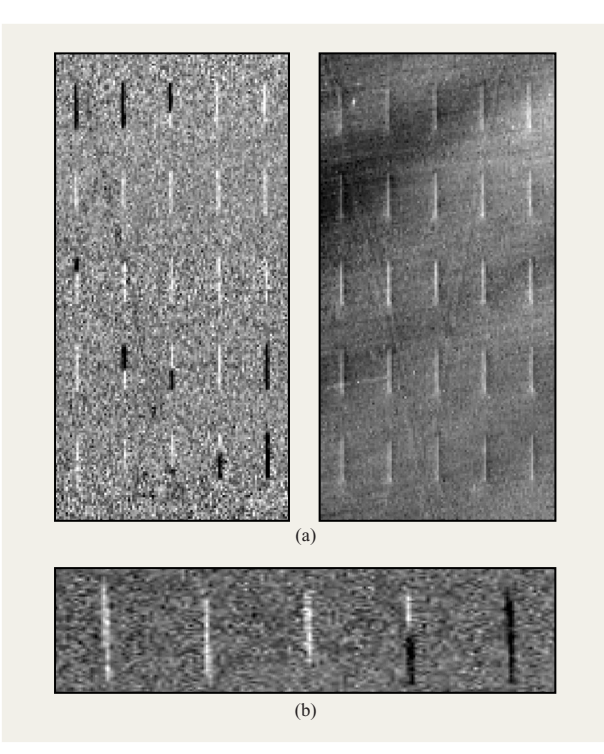
It is likely that irradiation-induced nucleation of a new structural phase is the mechanism responsible for the anisotropy changes observed in our Co/Pt film. Experience shows that it is easier to expand an already modified area than to create a new one. This agrees with the argument that nucleation of a new phase requires more energy than phase expansion. Whether this new phase is a modification of the Co film itself or of its interface is not yet clear to us. Both a reduced defect density within the film and a smoothed or intermixed interface are compatible with our

observations. Our results indicate that the substrate plays a minor role in this process. Structural modifications require more activation energy in the bulk than at the interface or in the film because the number of intrinsic defects is much lower in the substrate.

6. Microstructures

A natural extension of magnetism research in ultrathin films is to attempt to shrink the lateral sizes to produce small magnetic structures, which are confined in all three dimensions. The technological motivation behind magnetic patterning was mentioned in the preceding section: By limiting a magnetic bit to a structurally confined entity, the currently expected limits of longitudinal magnetic storage might be moved or bypassed. In particular, the transition noise between adjacent bits and the thermal instability of bits containing too few atoms are unsolved issues for the present scheme. In patterned media, transition noise is absent, and the number of spins in a bit could be kept sufficiently high by increasing the thickness of the small element.

Patterned magnetic media can be produced in various ways. The patterning of an ultrathin film by electron or ion irradiation was described in the preceding section. An



(a) Magnetization (left) and topography (right) of an array of 1 $\mu m \times 20~\mu m$ -sized Co/Cu(001) bars, imaged in the as-grown state. The Co thickness was 4 ML. The magnetization component along the bars was measured. The majority of the elements were single-domain, but six out of 25 bars decayed into a multidomain state. (b) Enlarged view of the bottom row of (a). The third and fourth bars from the left decayed into a multidomain state. The bottom part of the third bar was magnetized horizontally and hence appears gray.

alternative—and up to now more frequently used—method is to fabricate small magnetic entities separated from one another by lithographical means. For thick magnetic films (typically 10 nm and greater) this is achieved by electron-beam lithography [55, 56] or X-ray lithography [57]. In ultrathin films a few atomic layers thick, these techniques are applicable only if the films are protected against air, because of the subsequent lithography steps. For studying the intrinsic magnetic properties of ultrathin uncovered structures, a different approach is used: The patterns are produced by evaporation through shadow masks [58].

The questions posed by these ultrathin microstructures are manifold, and most of them are yet unsolved. Domain formation and magnetization reversal, for instance, must be thoroughly understood before patterned media will make their way into products. In a sense, the field of magnetic microstructures is in a state quite similar to the early days of ultrathin epitaxial films of infinite lateral

dimensions ten years ago. Conflicting results were reported at that time for most ferromagnetic thin-film systems, in particular because several growth parameters were not fully appreciated and thus the films varied strongly in quality. Similarly conflicting results are currently obtained for microstructures. Therefore, instead of presenting a comprehensive overview of domain formation, we cite only one example of the Co/Cu(001) model system to illustrate how spin-SEM contributes to this type of investigation.

As an extended ultrathin film, as-grown Co/Cu(001) has been shown to be in an in-plane magnetized single-domain state over lateral distances of a few millimeters [59]. Only after demagnetizing in an ac magnetic field do domains with irregular boundaries appear. The situation has been shown to be completely different in perpendicularly magnetized films such as Co/Au(111). For such films, a multidomain state has been observed [60]. It is not clear a priori what happens if the lateral size is reduced. In thick in-plane magnetized Fe(001) elements on GaAs, a transition from single-domain to multidomain remanent states is observed upon reducing the lateral size to less than 50 μm and is ascribed to the competition of in-plane dipolar and anisotropy fields [61]. Distinct micromagnetic structures arise according to the orientation of the element edges. On the other hand, since the magnetostatic energy becomes small for ultrathin films, the single-domain state encountered for an extended film might still be the energetically preferred one.

Figure 9 shows the as-grown magnetic state of an array of $1 \times 20 \ \mu\text{m}^2$ Co/Cu(001) bars 4 ML thick. Singledomain elements were found, as well as some having a random arrangement of two or more domains. For a fixed bar width, the number of domains increased with bar length. This finding is in striking contrast to a recent report stating that irrespective of shape, size, and applied field, no domains penetrate small Co/Cu(001) elements [62], but it agrees with the results of Oepen and coworkers [63]. The reason for this discrepancy in the asgrown ultrathin elements is unclear at the time of writing. One possibility is that structural defects can act as pinning sites, but this is also true for extended in-plane magnetized films, which do not break up into domains. For perpendicularly magnetized films, the situation is less complicated: A multidomain state is preferred for extended films as well as for element sizes down to the submicrometer level [57, 62].

The issue of domain formation in small structures is obviously more complex than anticipated. In particular, it is not even clear whether the as-grown, remanent, or demagnetized state better mimics the energy ground state. Experimentally we find that an as-grown multidomain state is converted to a single-domain state upon application of a large magnetic field pulse. Thereafter, the

remanent state of the bar remains single-domain even after repeated switching cycles. It is not yet known how the switching actually proceeds. For 35-nm-thick Ni bars, the dependence of the switching field on bar width suggests that quasi-coherent switching occurs in short bars, but incoherent switching occurs in long bars [55]. Again, the observed absence of a systematic trend with element geometry in Co/Cu(001) [62] remains puzzling.

Much more work is necessary to resolve these issues and to find the limits of ferromagnetic stability in ultrathin two-dimensional elements. In any case, speculations that only a few atoms forming a nanometer-sized dot may provide a stable magnetic bit for "nanorecording" [62] are not supported by experimental evidence, nor are they expected from thermodynamic considerations.

7. Ultrafast magnetization switching

The speed of magnetization reversal is a key feature in magnetic data storage. The data rate in longitudinal recording is currently 40 MB/s and continues to double every two years. This means that magnetization reversal takes place in times approaching one nanosecond. In all currently employed data storage schemes, the reversing field produced by the write head is applied in the opposite direction of the magnetization, and hence the torque exerted on the magnetization is minimal. This means that thermal fluctuations or local deviations from nominal material parameters can initiate reversal, as illustrated in Section 4 for the reversal in ultrathin Fe/Cu films. It has recently been shown, however, that reversal on a much shorter time scale is possible if the external magnetic field is applied perpendicularly to the magnetization [64, 65]. In this case, the magnetic field pulse induces a precession of the magnetization that leads to reversal. This reversal mode has been shown to occur on a picosecond time scale.

The experiment proving that reversal of magnetization is successfully initiated by a picosecond field pulse has been performed at the Stanford Linear Accelerator Center. Extremely short and intense electron pulses between 2 and 5 ps duration can be produced by utilizing the relativistic electron bunch of 46-GeV energy, which is laterally compressed to 3.8 μ m \times 0.8 μ m in size. The magnetic field associated with the moving charge reaches very high amplitudes of $>10^4$ kA/m near the center of the beam and falls off inversely with the distance from the center, according to Ampère's law. This beam impinges on a thin magnetic film, which is magnetically saturated along its easy magnetization direction. After exposing the sample to such an extreme field pulse, it is removed from the beamline and the recorded magnetization pattern is examined. Perpendicular as well as in-plane magnetized samples have been investigated, and both types show characteristic high-symmetry patterns of reversed regions around the impact location of the beam. Here we present in-plane magnetized epitaxial Co films of 20 nm thickness.

This example has been selected because in-plane films can be switched on a picosecond time scale with much smaller fields than those magnetized perpendicularly. This feature makes them attractive for new concepts in data storage. The strong reduction in field necessary to switch magnetization is due to the demagnetizing field brought about by the precession of the magnetization out of the film plane during the field pulse. This reduces the field amplitudes to values that are well within the reach of conventional thin-film recording heads [66].

Figure 10(a) shows the magnetic pattern generated in a uniaxial Co film by a single pulse of 4.4 ps duration. The location of impact is at the center of the image, which is defined as the center of the coordinate system. Originally the sample was premagnetized along the +y direction, color-coded as black in the figure. In the white areas, the magnetization has switched from +y to -y. Obviously a field pulse of 4.4 ps duration is sufficient to switch the magnetization at certain field values and at certain angles between external field and premagnetization. Note that the induced magnetization pattern is symmetric upon changing the sign of y, but asymmetric upon changing the sign of x.

The observed switching can be described as the solution of the Landau-Lifshitz equation

$$\frac{d\vec{M}}{dt} = -\gamma(\vec{M} \times \vec{H}_{\text{tot}}) + \frac{\alpha}{M} \left(\vec{M} \times \frac{d\vec{M}}{dt} \right). \tag{2}$$

According to this equation, the magnetization \vec{M} describes a damped precession around the direction of the sum of internal and external magnetic fields $\vec{H}_{\text{tot}} = \vec{H}_{\text{ex}} + \vec{H}_{\text{D}} + \vec{H}_{\text{A}}$, where \vec{H}_{ex} is the external pulse field, \vec{H}_{D} the demagnetizing field, and \vec{H}_{A} the anisotropy field. The gyromagnetic ratio is $\gamma = 0.2212 \times 10^6$ m/As, and the relaxation of \vec{M} into the field direction is described by the damping constant α .

Within this model, precessional reversal can be described in three steps: First, during the ultrafast field pulse, \vec{M} precesses around $\vec{H}_{\rm ex}$ out of the film plane. As \vec{M} leaves the plane of the film, the effective demagnetizing field increases with increasing angle θ between \vec{M} and the film plane: $H_{\rm D} = (M_{\rm s}/\mu_0) \sin \theta$. Then, when $\vec{H}_{\rm ex}$ ceases to exist, \vec{M} continues to precess, but now around $\vec{H}_{\rm D} + \vec{H}_{\rm A}$. The maximum angle θ assumed by \vec{M} determines whether the magnetization reverses and whether even multiple reversals can occur. Finally, \vec{M} eventually relaxes into one of the two easy magnetization directions. This final step takes up to several hundred picoseconds.

According to this model, the field for inducing precessional reversal is minimal along the directions where

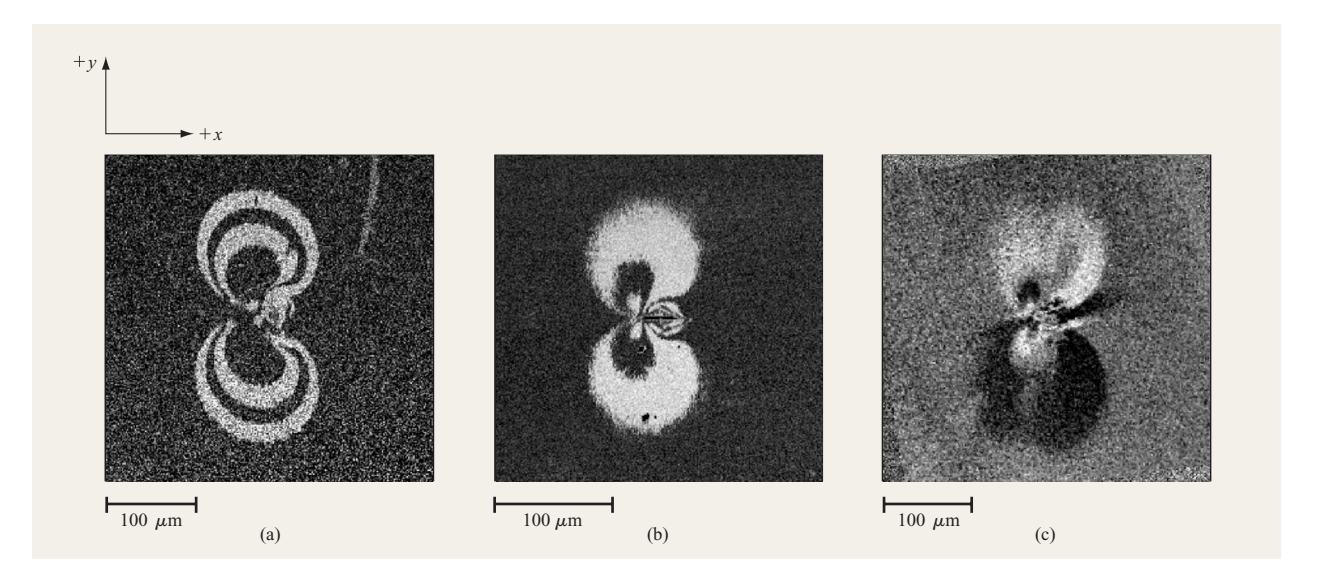


Figure 10

In-plane magnetization patterns written into three 20-nm Co films by a magnetic field pulse of 4.4-ps duration and subsequently imaged by spin-SEM (each was premagnetized along the +y direction): (a) Uniaxial Co film grown on a MgO(110) substrate with an Fe/Pt buffer. The magnetization component along the y axis has been measured. In the black areas, the magnetization points in the original +y direction; in the white areas, it has reversed to the -y direction. (b) Uniaxial Co film grown on a MgO(110) substrate with a Cr/Pt buffer. The magnetization component along the y axis has been measured. (c) Co film grown on a MgO(100) substrate with a Cr/Pt buffer. The magnetic anisotropy contains a uniaxial and a fourfold symmetric in-plane component. The magnetization component along the x axis has been measured; i.e., in the black areas the magnetization points in the -x direction, in the white areas in the +x direction. The background has no x component of magnetization and hence appears gray.

the torque $\vec{H}_{ex} \times \vec{M}$ is maximal, i.e., where $\vec{H}_{ex} \perp \vec{M}$. Experimentally this is indeed observed, as indicated in Figure 10(a) along the line x = 0. A first reversal occurs at a radius of 110 μ m from the center, corresponding to a field of only 184 kA/m. Toward y = 0, i.e., toward larger field values, multiple reversals occur, corresponding to a precessional motion encompassing an angle that is an odd multiple of π . On the line with zero torque, y = 0, no reversal is observed outside the area of beam damage. This shows the fundamental difference between conventional magnetization reversal with \vec{H}_{ex} antiparallel to \vec{M} and precessional reversal. In the case of precessional reversal, the torque is nonzero. No fundamental limit appears to exist for the time interval over which the magnetic field must be applied to induce reversal. In conventional magnetization reversal, on the other hand, the torque equals zero. In this case, the angular momentum induced by the reversal process must be absorbed by the phonon lattice, a process that is governed by the rate of energy exchange between the magnetic system and the lattice. Therefore the relevant ultimate time scale for conventional reversal is the spin lattice relaxation time, which is of the order of 100 ps [67].

According to Equation (2), the precessional motion of the magnetization is damped. The damping constant α is material-dependent. Hence, the minimum field necessary for reversal as well as the ability to exhibit multiple reversals depends on the sample properties. Figure 10(b) shows the magnetic pattern generated in a Co film grown with essentially the same magnetic properties. Structurally the films differ because they were grown on different buffer layers. The precessional reversal in both these films can be described by the same set of magnetic parameters, but with a damping constant differing by almost one order of magnitude: $\alpha = 0.037$ for the film in Figure 10(a), and $\alpha = 0.22$ for the one in Figure 10(b) [68]. Finally, Figure 10(c) shows the magnetic pattern generated in a Co film with the same growth properties as the one shown in Figure 10(b) but containing both twofold and fourfold symmetric anisotropy contributions. The induced pattern clearly reflects the underlying symmetry: Although the shape of the magnetic pattern is still symmetric with respect to the y axis, the magnetization itself is antisymmetric.

The examples presented in Figure 10 show that precessional magnetization reversal can be induced by picosecond field pulses of moderate amplitude in in-plane

magnetized thin films. In contrast to perpendicularly magnetized films, the demagnetizing field supports precessional reversal. Therefore, in-plane magnetized films with low damping constants are promising candidates for entirely different data storage concepts that are based on writing data by exploiting magnetization precession.

8. Concluding remarks

The objective of this paper was to illustrate the capabilities of an advanced microscopy technique for magnetization mapping: spin-SEM. The technique has been described, including its main strengths and weaknesses. The various examples presented in this review are not meant to be representative of the impact which the method has made on bulk and thin-film magnetism. Rather, they were chosen to illustrate the primary features that differentiate this technique from alternative methods to investigate magnetization patterns. These examples embrace both fundamental and technologically relevant aspects of ferromagnetism in thin films.

We have examined examples of the separation of magnetic and structural information, of high-resolution domain wall imaging, and of the capability of the technique to image magnetization patterns not only on flat but also on inclined surfaces. The extreme surface sensitivity of the technique has been illustrated by the visualization of the magnetization reversal in an ultrathin film. Technologically relevant aspects have been addressed by an original approach to the patterning of magnetic media directly with an electron beam. The investigation of laterally confined magnetic structures and the initiation of magnetization reversal by field pulses much shorter than those currently used in write heads of magnetic data storage devices have also been covered.

I am aware that some fascinating topics have been omitted from the present discussion. Most prominently, magnetic multilayers have not been discussed. Spin-SEM has contributed to the study of exchangecoupled bilayers by allowing the direct visualization of ferromagnetic/antiferromagnetic coupling across spacer layers and high-precision measurements of relevant oscillation periods [69]. I have not discussed the domain formation at the spin reorientation transition [70, 71], nor temperature-dependent domain studies to identify the prominent role of thermodynamic fluctuations in two dimensions. Technological applications range from the investigation of domain patterns in amorphous soft magnetic materials to magnetic storage devices. The magnetic bits in longitudinal recording are shrinking at an incredible pace, but spin-SEM is still able to image such small patterns [24].

All of these investigations benefit from the fact that spin-SEM combines the following attractive features: higher spatial resolution than conventional reflection-type imaging techniques, high surface sensitivity, quantitative determination of the magnetization direction, and a clear discrimination between the simultaneously mapped topographical and magnetic images.

Acknowledgments

The magnetism project at the IBM Zurich Research Laboratory would not have been possible without the valuable contributions of many individuals. In particular, the author gratefully acknowledges his colleague Andi Bischof for his major contributions over more than a decade to the design and construction of the experimental system used in this work, as well as for keeping it running. The experimental data presented in this paper were taken in collaboration with Michele Stampanoni, Wolfgang Weber, Jürgen Fassbender, Urs Dürig, Peter Grütter, Christian Back, and Hans-Christoph Siegmann.

References

- 1. P. Weiss, "L'Hypothèse du Champ Moléculaire et la Propriété Ferromagnétique," *J. de Physique* **6,** 661 (1907).
- F. Bitter, "On Inhomogeneities in the Magnetization of Ferromagnetic Materials," *Phys. Rev.* 38, 1903–1908 (1931).
- L. von Hámos and P. A. Thiessen, "Über die Sichtbarmachung von Bezirken verschiedenen ferromagnetischen Zustandes fester Körper," Z. Phys. 71, 442–444 (1931).
- H. J. Williams and W. Shockley, "A Simple Domain Structure in an Iron Crystal Showing a Direct Correlation with the Magnetization," *Phys. Rev.* 75, 178–183 (1949).
- A. Hubert and R. Schäfer, Magnetic Domains, Springer, Berlin, 1998.
- K. Koike, H. Matsuyama, and K. Hayakawa, "Spin-Polarized Scanning Electron Microscopy for Micro-Magnetic Structure Observation," *Scan. Microsc.* 1, 241–253 (1987).
- G. G. Hembree, J. Unguris, R. J. Celotta, and D. T. Pierce, "Scanning Electron Microscopy with Polarization Analysis: High Resolution Images of Magnetic Microstructure," Scan. Microsc. 1, 229–240 (1987).
- 8. H. P. Oepen and J. Kirschner, "Imaging of Magnetic Microstructures at Surfaces: The Scanning Electron Microscope with Spin Polarization Analysis," *Scan. Microsc.* 5, 1–16 (1991).
- R. Allenspach, "Ultrathin Films: Magnetism on the Microscopic Scale," J. Magn. Magn. Mater. 129, 160–185 (1994).
- T. H. DiStefano, "Technology for Detecting Small Magnetic Domains and Beam-Addressed Memory Therewith," *IBM Tech. Disclosure Bull.* 20, 4212–4215 (1978).
- K. Koike and K. Hayakawa, "Scanning Electron Microscope Observation of Magnetic Domains Using Spin-Polarized Secondary Electrons," *Jpn. J. Appl. Phys.* 23, L187–L188 (1984).
- J. Unguris, G. Hembree, R. J. Celotta, and D. T. Pierce, "High Resolution Magnetic Microstructure Imaging Using Secondary Electron Spin Polarization Analysis in a Scanning Electron Microscope," J. Microsc. 139, RP1–RP2 (1985).
- 13. J. Kessler, Polarized Electrons, Springer, Berlin, 1985.
- J. Kirschner, Polarized Electrons at Surfaces, Springer, Berlin, 1985.

- 15. M. R. Scheinfein, J. Unguris, M. H. Kelley, D. T. Pierce, and R. J. Celotta, "Scanning Electron Microscopy with Polarization Analysis (SEMPA)," Rev. Sci. Instrum. 61, 2501-2526 (1990).
- 16. D. P. Pappas, C. R. Brundle, and H. Hopster, "Reduction of Macroscopic Moment in Ultrathin Fe Films as the Magnetic Orientation Changes," Phys. Rev. B 45, 8169-8172 (1992).
- 17. D. L. Abraham and H. Hopster, "Magnetic Probing Depth in Spin-Polarized Secondary-Electron Spectroscopy," Phys. Rev. Lett. 58, 1352-1354 (1987).
- H. P. Oepen and J. Kirschner, "Magnetization Distribution of 180° Domain Walls at Fe(100) Single-Crystal Surfaces," Phys. Rev. Lett. 62, 819-822 (1989).
- 19. M. R. Scheinfein, J. Unguris, R. J. Celotta, and D. T. Pierce, "Influence of the Surface on Magnetic Domain-Wall Microstructure," Phys. Rev. Lett. 63, 668-671 (1990).
- 20. T. Duden and E. Bauer, "Spin-Polarized Low Energy Electron Microscopy of Ferromagnetic Layers," J. Electron Microsc. 47, 379-385 (1998).
- 21. J. Stöhr, Y. Wu, B. D. Hermsmeier, M. G. Samant, G. R. Harp, S. Koranda, D. Dunham, and B. P. Tonner, "Element-Specific Magnetic Microscopy with Circularly Polarized X-Rays," Science 259, 658-661 (1993).
- 22. C. M. Schneider, K. Holldack, M. Kinzler, M. Grunze, H. P. Oepen, F. Schafers, H. Petersen, K. Meinel, and J. Kirschner, "Magnetic Spectromicroscopy from Fe(100)," Appl. Phys. Lett. 63, 2432-2434 (1993).
- 23. J. Stöhr and S. Anders, "X-Ray Spectro-Microscopy of Complex Materials and Surfaces," IBM J. Res. Develop. 44, 535-551 (2000, this issue).
- 24. H. Matsuyama and K. Koike, "Twenty nm Resolution Spin Polarized Scanning Electron Microscope," J. Electron Microsc. (Japan) 43, 157-163 (1994).
- 25. R. Allenspach and M. Stampanoni, "Magnetic Domain Imaging of Epitaxial Thin Films by Spin-Polarized Scanning Electron Microscopy," Mater. Res. Soc. Symp. Proc. 231, 17-26 (1992).
- 26. S. Middelhoek, "Domain Walls in Thin Ni-Fe Films," J. Appl. Phys. 34, 1054–1059 (1963).
- 27. Y. Martin and H. K. Wickramasinghe, "Magnetic Imaging by 'Force Microscopy' with 1000 Å Resolution," Appl. Phys. Lett. 50, 1455-1457 (1987).
- 28. P. Kasiraj, R. M. Shelby, J. S. Best, and D. E. Horne, "Magnetic Domain Imaging with a Scanning Kerr Effect Microscope," IEEE Trans. Magn. MAG-22, 837-839 (1986).
- 29. H. Matsuyama, K. Koike, T. Kobayashi, R. Nakatani, and K. Yamamoto, "Side Plane Domain Observation of Fe-C/Ni-Fe/BN Multilayers with a Spin-Polarized Scanning Electron Microscope," Appl. Phys. Lett. 57, 2028-2030 (1990).
- 30. C. Schönenberger and S. F. Alvarado, "Understanding Magnetic Force Microscopy," Z. Phys. B 80, 373–383 (1990).
- 31. D. Rugar, H. J. Mamin, P. Guethner, S. E. Lambert, J. E. Stern, I. McFadyen, and T. Yogi, "Magnetic Force Microscopy: General Principles and Application to Longitudinal Recording Media," J. Appl. Phys. 68, 1169-1183 (1990).
- 32. G. Matteucci, M. Muccini, and U. Hartmann, "Flux Measurements on Ferromagnetic Microprobes by Electron Holography," *Phys. Rev. B* **50**, 6823–6828 (1994).

 33. W. Brown, "Virtues and Weaknesses of the Domain
- Concept," Rev. Mod. Phys. 17, 15-19 (1945).
- 34. E. C. Stoner and E. P. Wohlfarth, "A Mechanism of Magnetic Hysteresis in Heterogeneous Alloys," Phil. Trans. Roy. Soc. A 240, 599-642 (1948).
- 35. F. E. Luborsky, "Development of Elongated Particle Magnets," J. Appl. Phys. 32, 171S-183S (1961).
- 36. J. Pommier, P. Meyer, G. Pénissard, J. Ferré, P. Bruno, and D. Renard, "Magnetization Reversal in Ultrathin

- Ferromagnetic Films with Perpendicular Anisotropy: Domain Observations," Phys. Rev. Lett. 65, 2054–2057 (1990).
- 37. S. T. Purcell, M. T. Johnson, N. W. E. McGee, J. J. de Vries, W. B. Zeper, and W. Hoving, "Local Structural and Polar Kerr Effect Measurements on an Ultrathin Epitaxial Co Wedge Grown on Pd(111)," J. Appl. Phys. 73, 1360-1367
- 38. N. W. E. McGee, M. T. Johnson, J. J. de Vries, and J. aan de Stegge, "Localized Kerr Study of the Magnetic Properties of an Ultrathin Epitaxial Co Wedge Grown on Pt(111)," J. Appl. Phys. 73, 3418-3425 (1993).
- 39. S. Lemerle, J. Ferré, C. Chappert, V. Mathet, T. Giamarchi, and P. Le Doussal, "Domain Wall Creep in an Ising Ultrathin Magnetic Film," Phys. Rev. Lett. 80, 849-852 (1998).
- 40. P. Beauvillain, A. Bounouh, C. Chappert, R. Mégy, S. Ould-Mahfoud, J. P. Renard, and P. Veillet, "Effect of Submonolayer Coverage on Magnetic Anisotropy of Ultrathin Cobalt Films M/Co/Au(111) with M = Au, Cu, Pd," J. Appl. Phys. 76, 6078-6080 (1994).
- 41. M. Speckmann, H. P. Oepen, and H. Ibach, "Magnetic Domain Structures in Ultrathin Co/Au(111): On the Influence of Film Morphology," Phys. Rev. Lett. 75, 2035-2038 (1995)
- 42. W. Weber, C. H. Back, U. Ramsperger, A. Vaterlaus, and R. Allenspach, "Submonolayers of Adsorbates on Stepped Co/Cu(100): Switching of the Easy Axis," Phys. Rev. B 52, R14400-R14403 (1995).
- 43. S. Hope, E. Gu, B. Choi, and J. A. C. Bland, "Spin Engineering in Ultrathin Cu/Co/Cu(110)," Phys. Rev. Lett. **80,** 1750–1753 (1998)
- 44. R. J. Pollard, M. J. Wilson, and P. J. Grundy, "Interface Processing in Multilayer Films," J. Appl. Phys. 76, 6090-6092 (1994).
- 45. W. Weber, C. H. Back, A. Bischof, D. Pescia, and R. Allenspach, "Magnetic Switching in Cobalt Films by Adsorption of Copper," Nature 374, 788-790 (1995).
- 46. C. Chappert, H. Bernas, J. Ferré, V. Kottler, J. P. Jamet, Y. Chen, E. Cambril, F. Rousseaux, V. Mathet, and H. Launois, "Planar Patterned Magnetic Media Obtained by Ion Irradiation," Science 280, 1919-1922 (1998).
- 47. E. Grochowski and D. A. Thompson, "Outlook for Maintaining Areal Density Growth in Magnetic Recording," IEEE Trans. Magn. 30, 3797-3800 (1994).
- 48. R. Allenspach, A. Bischof, U. Dürig, and P. Grütter, "Local Modification of Magnetic Properties by an Electron Beam," Appl. Phys. Lett. 73, 3598-3600 (1998).
- 49. B. Kaplan and G. Gehring, "The Domain Structure in Ultrathin Magnetic Films," J. Magn. Magn. Mater. 128, 111-116 (1993).
- 50. C.-H. Chang and M. H. Kryder, "Effect of Substrate Roughness on Microstructure, Uniaxial Anisotropy, and Coercivity of Co/Pt Multilayer Thin Films," J. Appl. Phys. **75**, 6864–6866 (1994).
- 51. S. O. Demokritov, J. A. Wolf, and P. Grünberg, "Interfacial Reconstruction and Short-Period Oscillatory Coupling in Fe/Cr/Fe Multilayers after Electron Bombardment," Appl. Phys. Lett. 63, 2147-2149 (1993).
- 52. D. Weller, H. Brändle, and C. Chappert, "Relationship Between Kerr Effect and Perpendicular Magnetic Anisotropy in $Co_{1-x}Pt_x$ and $Co_{1-x}Pd_x$ Alloys," *J. Magn. Magn. Mater.* **121,** 461–470 (1993).
- 53. J. S. Tsay and C. S. Shern, "Diffusion and Alloy Formation of Co Ultrathin Films on Pt(111)," J. Appl. Phys. 80, 3777–3781 (1996).
- 54. L. Reimer and G. Pfefferkorn, Raster-Elektronenmikroskopie, Springer, Berlin, 1973.
- 55. S. Y. Chou, P. R. Krauss, and L. Kong, "Nanolithographically Defined Magnetic Structures and Quantum Magnetic Disk," J. Appl. Phys. 79, 6101-6106 (1994).

- R. M. H. New, R. F. W. Pease, and R. L. White, "Submicron Patterning of Thin Cobalt Films for Magnetic Storage," J. Vac. Sci. Technol. B 12, 3196–3201 (1994).
- M. Hehn, K. Ounadjela, J.-P. Bucher, F. Rousseaux, D. Decanini, B. Bartenlian, and C. Chappert, "Nanoscale Magnetic Domains in Mesoscopic Magnets," *Science* 272, 1782–1785 (1996).
- 58. J. L. Robbins, R. J. Celotta, J. Unguris, D. T. Pierce, B. T. Jonker, and G. A. Prinz, "Domain Images of Ultrathin Fe Films on Ag(100)," *Appl. Phys. Lett.* **52**, 1918–1920 (1988).
- H. P. Oepen, M. Benning, H. Ibach, C. M. Schneider, and J. Kirschner, "Magnetic Domain Structure in Ultrathin Cobalt Films," *J. Magn. Magn. Mater.* 86, L137–L142 (1990).
- R. Allenspach, M. Stampanoni, and A. Bischof, "Magnetic Domains in Thin Epitaxial Co/Au(111) Films," *Phys. Rev. Lett.* 65, 3344 (1990).
- 61. E. Gu, E. Ahmad, S. J. Gray, C. Daboo, J. A. C. Bland, L. M. Brown, M. Rührig, A. J. Gibbon, and J. N. Chapman, "Micromagnetism of Epitaxial Fe(001) Elements on the Mesoscale," *Phys. Rev. Lett.* 78, 1158–1161 (1997).
- C. Stamm, F. Marty, A. Vaterlaus, V. Weich, S. Egger, U. Maier, U. Ramsperger, H. Fuhrmann, and D. Pescia, "Two-Dimensional Magnetic Particles," *Science* 282, 449-451 (1998).
- 63. W. Lutzke, H. P. Oepen, and J. Kirschner, "Magnetic Domains in Micron-Scale Co Structures on Cu(001)," presented at the Third International Symposium on Metallic Multilayers (MML '98), Vancouver, June 14–19, 1998.
- 64. H. C. Siegmann, E. L. Garwin, C. Y. Prescott, J. Heidmann, D. Mauri, D. Weller, R. Allenspach, and W. Weber, "Magnetism with Picosecond Field Pulses," J. Magn. Magn. Mater. 151, L8-L12 (1995).
- C. H. Back, D. Weller, J. Heidmann, D. Mauri,
 D. Guarisco, E. L. Garwin, and H. C. Siegmann,
 "Magnetization Reversal in Ultrashort Magnetic Field Pulses," *Phys. Rev. Lett.* 81, 3251–3254 (1998).
- R. Wood, M. Williams, and J. Hong, "Considerations for High Data Rate Recording with Thin-Film Heads," *IEEE Trans. Magn.* 26, 2954–2959 (1990).
- A. Vaterlaus, T. Beutler, D. Guarisco, M. Lutz, and F. Meier, "Spin-Lattice Relaxation in Ferromagnets Studied by Time-Resolved Spin-Polarized Photoemission," *Phys. Rev. B* 46, 5280–5286 (1992).
- 68. C. H. Back, R. Allenspach, W. Weber, S. S. P. Parkin, D. Weller, E. L. Garwin, and H. C. Siegmann, "Minimum Field Strength in Precessional Magnetization Reversal," *Science* 285, 864–867 (1999).
- J. Unguris, R. J. Celotta, and D. T. Pierce, "Observation of Two Different Oscillation Periods in the Exchange Coupling of Fe/Cr/Fe(100)," *Phys. Rev. Lett.* 67, 140–143 (1991).
- R. Allenspach and A. Bischof, "Magnetization Direction Switching in Fe/Cu(100) Epitaxial Films: Temperature and Thickness Dependence," *Phys. Rev. Lett.* 69, 3385–3388 (1992).
- H. P. Oepen, M. Speckmann, Y. Millev, and J. Kirschner, "Unified Approach to Thickness-Driven Magnetic Reorientation Transitions," *Phys. Rev. B* 55, 2752–2755 (1997).

Received June 15, 1999; accepted for publication October 5, 1999

Rolf Allenspach IBM Research Division, Zurich Research Laboratory, CH-8803 Rüschlikon, Switzerland (ral@zurich.ibm.com). Dr. Allenspach studied physics at the Eidgenössische Technische Hochschule (ETH) in Zurich, Switzerland, and received a Ph.D. in 1986. His thesis pertained to the physical aspects of spin-polarized electron spectroscopies. Joining the IBM Zurich Research Laboratory as a Research Staff Member, he then started a project on the investigation of ultrathin magnetic films. At present he manages the "Transport and Magnetism in Layered Structures" project. Dr. Allenspach also lectures at ETH on topics in condensed-matter physics since having completed his habilitation in 1994. In 1992 he was elected Wohlfarth Lecturer by the Institute of Physics, London, and he received an IBM Outstanding Technical Achievement Award in 1994 for the development of a high-spatial-resolution spin-SEM and its application to the study of thin-film magnetism.